Journal of Molecular Cell Biology (2022), 14(5), mjac029 https://doi.org/10.1093/jmcb/mjac029
Publish online May 5, 2022

Article

Structural insights reveal the specific recognition of meiRNA by the Mei2 protein

Siyuan Shen[1,2,†], Yanze Jian[1,2,†], Zhaokui Cai[3], Fudong Li[1,2], Mengqi Lv[1,2], Yongrui Liu[1,2], Jihui Wu[1,2], Chuanhai Fu[1,2,*], and Yunyu Shi[1,2,*]

[1] School of Life Sciences, Division of Life Sciences and Medicine, University of Science and Technology of China, Hefei 230026, China
[2] MOE key Laboratory for Cellular Dynamics, University of Science & Technology of China, Hefei 230026, China
[3] Key Laboratory of RNA Biology, Institute of Biophysics, Chinese Academy of Sciences, Beijing 100101, China
[†] These authors contributed equally to this work.
* Correspondence to: Chuanhai Fu, E-mail: chuanhai@ustc.edu.cn; Yunyu Shi, E-mail: yyshi@ustc.edu.cn

Edited by Jiarui Wu

In the fission yeast *Schizosaccharomyces pombe,* Mei2, an RNA-binding protein essential for entry into meiosis, regulates meiosis initiation. Mei2 binds to a specific non-coding RNA species, meiRNA, and accumulates at the *sme2* gene locus, which encodes meiRNA. Previous research has shown that the Mei2 C-terminal RNA recognition motif (RRM3) physically interacts with the meiRNA 5′ region *in vitro* and stimulates meiosis *in vivo*. However, the underlying mechanisms still remain elusive. We first employed an *in vitro* crosslinking and immunoprecipitation sequencing (CLIP–seq) assay and demonstrated a preference for U-rich motifs of meiRNA by Mei2 RRM3. We then solved the crystal structures of Mei2 RRM3 in the apo form and complex with an 8mer RNA fragment, derived from meiRNA, as detected by *in vitro* CLIP–seq. These results provide structural insights into the Mei2 RRM3–meiRNA complex and reveal that Mei2 RRM3 binds specifically to the UUC(U) sequence. Furthermore, a structure-based Mei2 mutation, Mei2^{F644A} causes defective karyogamy, suggesting an essential role of the RNA-binding ability of Mei2 in regulating meiosis.

Keywords: Mei2, meiRNA, meiosis, RNA-binding protein, crystallography

Introduction

Meiosis is a specialized cellular process that exists in a wide range of eukaryotic organisms, generating haploid gametes from diploid cells. Despite its important biological function, the molecular mechanisms that underlie meiosis remain elusive, particularly the regulation of meiotic initiation. The fission yeast *Schizosaccharomyces pombe* is an ideal model system to study the regulatory mechanisms of meiotic initiation (Yamamoto, 1996a). In recent years, remarkable progress has been made in understanding the switch from mitosis to meiosis in *S. pombe* (Watanabe and Yamamoto, 1994). Mei2, an RNA-binding protein encoded by the *mei2* gene (Shimoda et al., 1987), and a long non-coding meiRNA play critical roles in the initiation and progression of meiosis in *S. pombe* (Yamamoto, 1996b).

The Pat1 protein kinase phosphorylates Mei2 in mitotically growing cells, and the RNA-binding activity of Mei2 is suppressed (Watanabe et al., 1997; Yamanaka et al., 2010; Otsubo et al., 2014). Upon nutrient starvation, the kinase activity of Pat1 is suppressed, and an HMG-type transcription factor, Ste11, enhances the expression of Mei2 and up-regulates the transcription of meiRNA (Watanabe et al., 1988; Kitamura et al., 2001; Mata and Bahler, 2006; Yamashita et al., 2017). Therefore, the increased amount of Mei2 in its active form could interact with meiRNA (Yamashita et al., 1998; Sato et al., 2001) to form a dot structure called Mei2 dot, which co-localizes with the chromosomal locus of the *sme2* gene, from which meiRNA is transcribed (Chikashige et al., 1994; Chikashige et al., 1997; Shimada et al., 2003).

The Mei2 dot plays a pivotal role in the mitosis–meiosis switch. Mmi1 is sequestered to this dot so that meiosis-specific transcripts become free from Mmi1-dependent mRNA elimination (Stoilov et al., 2002; Yamamoto, 2010). During vegetative growth, the transcription of *S. pombe* meiotic genes is not completely repressed. These meiosis-specific transcripts include *mei4*, *ssm4*, *rec8*, and *spo5*, which encode factors required for proper progression of meiosis (Yamashita et al., 1997; Horie et al., 1998; Watanabe and Nurse, 1999; Niccoli et al., 2004). *S. pombe* utilizes selective elimination machinery to remove the mistimed expression of meiotic gene

Received January 24, 2022. Revised April 5, 2022. Accepted April 13, 2022.

transcripts. Mmi1 plays an indispensable role in this process. Mmi1 interacts with the determinant of selective removal (DSR) element on the gametogenic gene transcripts through a C-terminal YTH domain (Harigaya et al., 2006; Yamanaka et al., 2010). It also associates with the nuclear RNA elimination factor Erh1 via its N-terminus to promote facultative heterochromatin assembly and repress the expression of gametogenic genes (Zofall et al., 2012; Sugiyama et al., 2016; Shichino et al., 2018; Xie et al., 2019). Since Mmi1 suppresses the expression of meiotic genes, it should be inactivated when cells proceed to meiosis, and upon entering meiosis, the Mei2 dot blocks the function of the DSR–Mmi1 RNA elimination system. The meiRNA contains numerous copies of the DSR motif in its 3′ region and acts as a decoy for Mmi1 (Shichino et al., 2014). Mmi1 interacts with the DSR motif of the meiRNA 3′ region and is thereby sequestered to the Mei2 dot. Hence, meiotic transcripts are shielded from Mmi1-dependent mRNA elimination and can function stably to ensure the reliable operation of the mitosis–meiosis switch (Harigaya and Yamamoto, 2007; Emsley et al., 2010).

Although the mechanism by which the YTH domain of Mmi1 recognizes the DSR motif is well understood (Wang et al., 2016; Wu et al., 2017), how Mei2 protein recognizes meiRNA remains unclear. To investigate this issue, we first used crosslinking and immunoprecipitation sequencing (CLIP–seq) experiments and fluorescent polarization (FP) assays *in vitro* to identify an 8mer meiRNA fragment that directly engages the Mei2 C-terminal RNA recognition motif (RRM3). We then determined a 1.9 Å crystal structure of the Mei2 RRM3 domain and a 2.35 Å resolution crystal structure of Mei2 RRM3 in complex with the 8mer meiRNA fragment. Using structural analyses, we identified the key residues of Mei2 RRM3 that are responsible for the specific recognition of meiRNA. We found that Mei2 RRM3 interacted in a sequence-specific manner with a UUC(U) motif of meiRNA. The structure-based mutation, Mei2^{F644A}, in Mei2 RRM3 results in fewer zygotes and defective karyogamy. Using a combination of biochemical, structural, and functional studies, we revealed the mechanism of the specific recognition of a UUC(U) motif of meiRNA by the Mei2 RRM3 domain. These findings underscore the importance of the meiRNA–Mei2 dot structure in the cell cycle switch from mitosis to meiosis in *S. pombe*.

Results

The structure of S. pombe Mei2 RRM3 domain

Previous studies have revealed that Mei2 mainly utilizes its C-terminal RRM3 to interact with meiRNA (Figure 1A; Watanabe et al., 1997). To understand the molecular structure of the Mei2 RRM3 domain, we chose to use a fragment (amino acid residues 580–733), which is evolutionarily conserved based on a sequence alignment of Mei2 (Figure 1B), for further experimentation. We determined a 1.9 Å resolution crystal structure of the yeast Mei2 RRM3 domain (PDB ID: 7EIO). The structure was solved by single wavelength anomalous scattering phasing on Se atoms using selenomethionine (SeMet)-labelled Mei2 RRM3 (Table 1). The crystals belong to the $P4_1$ space group and include two molecules in an asymmetric unit. In the final model, most Mei2 RRM3 residues, amino acid residues 580–725 for molecule A and amino acid residues 580–725 for molecule B, could be unambiguously built, except for several very C-terminal residues, probably due to flexibility at this position (Supplementary Figure S1A). The two molecules are highly similar, with a root-mean-square deviation (rmsd) of 0.284 Å for Cα atoms (127 atoms to 127 atoms). The structure shows that Mei2 RRM3 contains a core RRM fold similar to the canonical RRM, with a four-stranded β-sheet and two α-helixes (Figure 1B; Supplementary Figure S1B). The core βαββαβ is extended at the C-terminus by an additional α-helix (αC) and β-sheet (βC) and at the N-terminus by an extra α-helix (αN) (Figure 1C and D). The β-sheet surface is predominantly positively charged, providing a suitable interface for RNA binding (Figure 1E). The aliphatic side chains and aromatic rings lying on the β-sheet surface form a conserved hydrophobic core, suggesting possible RNA binding.

Mei2 RRM3 prefers to recognize U-rich RNA sequences

Mei2 RRM3 plays an essential role in the initiation of yeast meiosis. However, like many RNA–protein complexes, its recognition sites for meiRNA are poorly understood. We first evaluated the meiRNA-binding potential of Mei2 RRM3 by performing electrophoretic mobility shift assay (EMSA) experiments with meiRNA (1–508 nt). Previous studies have reported that Mei2 binds specifically to this molecule both *in vivo* and *in vitro* (Watanabe and Yamamoto, 1994). As expected, our EMSA result revealed that Mei2 RRM3 can interact with meiRNA (1–508 nt) *in vitro* (Supplementary Figure S2A). Next, we employed an *in vitro* CLIP–seq assay to map the binding region of meiRNA by Mei2 RRM3 (Supplementary Figure S2B). The binding showed a pervasive mode but with four obvious peaks (Figure 2A; Supplementary Figure S2C). Sequence alignment and WebLogo (https://weblogo.berkeley.edu/logo.cgi) analysis of the sequences of the four binding peaks demonstrated that Mei2 RRM3 prefers a U-rich sequence (Figure 2B). According to the result of sequence alignment and WebLogo analysis, we selected three different-length meiRNA fragments of the CLIP–seq-identified peak_1 (20mer meiRNA 5′-GUCAAUCUUCUGCCGUCUUG-3′, 12mer meiRNA 5′-UCAAUCUUCUGC-3′, and 8mer meiRNA 5′-UCUUCUGC-3′) for FP assay. We found that Mei2 RRM3 displayed similar binding to 20mer, 12mer, and 8mer meiRNA at dissociation constant (K_D) values of about 0.73 μM, 0.31 μM, and 0.53 μM, respectively (Figure 2C). The FP assay result suggests that 8mer meiRNA containing a conserved U-rich motif plays an indispensable role in the CLIP–seq-identified meiRNA region in Mei2 binding. Generally, CLIP–seq studies and FP assays of meiRNA-binding sites *in vitro* established that the Mei2 RRM3 domain preferred binding to U-rich RNA motifs.

The structure of Mei2 RRM3 in complex with 8mer meiRNA

According to the FP assay result, we chose to use 8mer meiRNA for further experiments. To provide a structural basis for

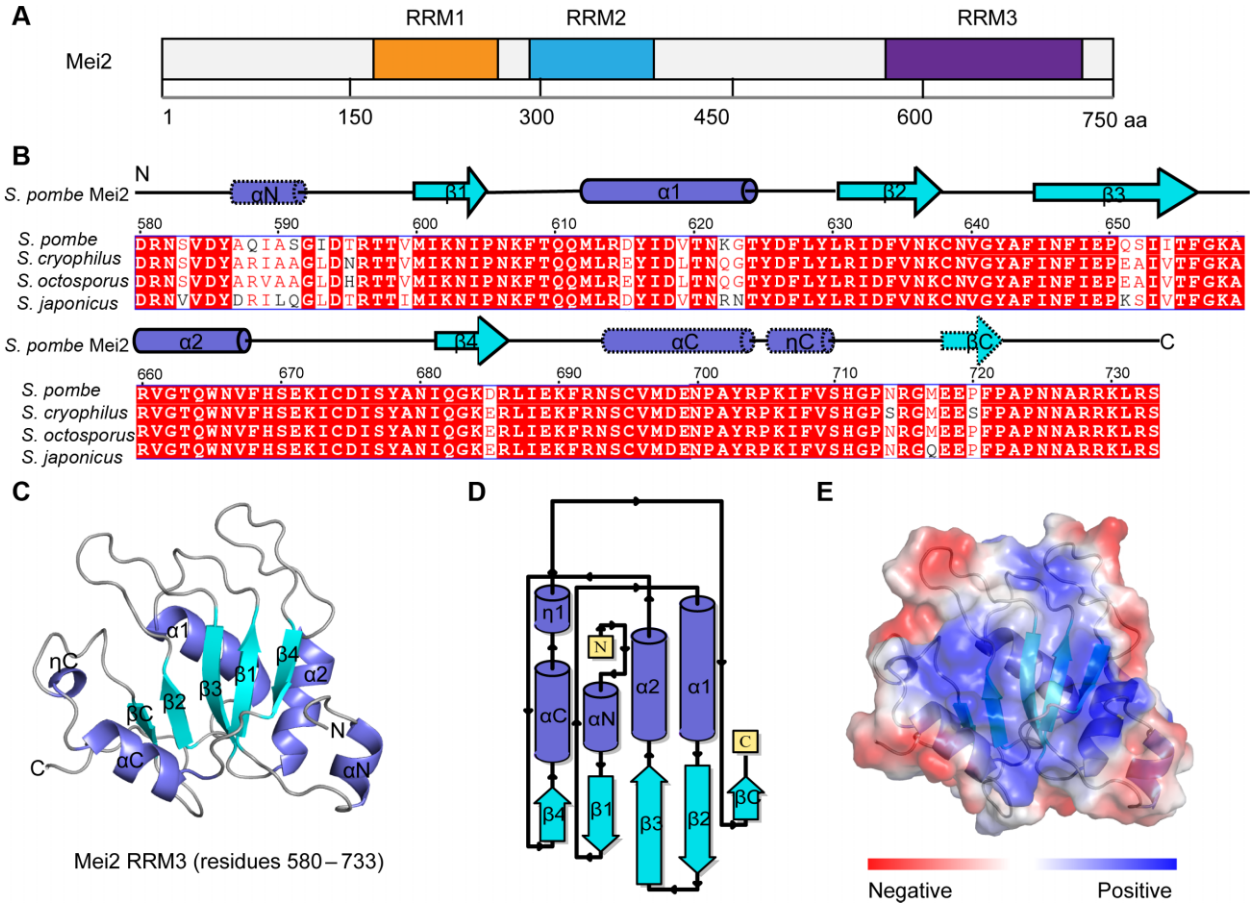

Figure 1 Crystal structure of Mei2 RRM3 protein. (**A**) Domain organization of the *S. pombe* Mei2 protein. (**B**) Sequence alignment of Mei2 RRM3 proteins from *S. pombe*, *S. cryophilus*, *S. octosporus*, and *S. japonicus*. The alignment was generated by ESPript3 with CLUSTALW (red squares, identical residues). Secondary structural elements of Mei2 RRM3 are shown above the sequences. Mei2 RRM3 comprises a single RRM domain (β1–α1–β2–β3–α2–β4), flanked by N-terminal (αN) and C-terminal regions (αC–ηC–βC). (**C**) Ribbon representation of Mei2 RRM3. β-sheets are colored in cyan, and α-helices are colored in slate. (**D**) Topological graph of Mei2 RRM3. β-sheets are colored in cyan, and α-helices are colored in slate. (**E**) Electrostatic surface potential map of Mei2 RRM3. Red and blue colors denote negative and positive surface charges, respectively.

understanding target RNA recognition by Mei2 RRM3, we determined a 2.35-Å-resolution crystal structure of Mei2 RRM3 in complex with 8mer meiRNA (5′-$U^1C^2U^3U^4C^5U^6G^7C^8$-3′) containing a central U-rich segment (PDB ID: 7EIU). The crystal belongs to the $C222_1$ space group, and the asymmetric unit contains two RRM3 domains, each binding to an RNA molecule, respectively (Supplementary Figure S3A; Table 1). In the final model, most of the Mei2 RRM3 protein residues and the 8mer meiRNA (5′-$U^3U^4C^5U^6G^7C^8$-3′) nucleotides could be unambiguously built, with the electron density of only a few C-terminal residues of Mei2 RRM3 and the 5′ terminal U^1C^2 of 8mer meiRNA being invisible, probably due to their flexibility. Supplementary Figure S3B shows the *2Fo-Fc* electron density map for 8mer meiRNA (5′-$U^3U^4C^5U^6G^7C^8$-3′). To test whether the invisible 5′ terminal U^1C^2 is required for the binding, we measured the binding affinity of Mei2 RRM3 with 6mer meiRNA (5′-$U^3U^4C^5U^6G^7C^8$-3′) by FP assay. The K_D value of Mei2 RRM3 toward 6mer meiRNA (5′-$U^3U^4C^5U^6G^7C^8$-3′) is 0.61 ± 0.03 μM, which is similar to that toward 8mer meiRNA (0.53 ± 0.02 μM) (Supplementary Figure S3C). This result suggests that 5′ terminal U^1C^2 plays a dispensable role in the Mei2 RRM3–meiRNA interaction. The Mei2 RRM3's overall structure and domain orientation, in complex with 8mer meiRNA, is similar to the unbound structure arrangement with an rmsd of 0.272 Å. In the structure, meiRNA (5′-$U^3U^4C^5U^6G^7C^8$-3′) mainly bound on the β-sheet surface and the loop joining β4 and αC (called the β4–αC loop) of the Mei2 RRM3 domain (Figure 3A). Although most nucleotides of 8mer meiRNA could be traced, only 5′-$U^3U^4C^5$-3′ of these nucleotides interacted with Mei2 RRM3, and 520 $Å^2$ of the surface was buried between Mei2 RRM3 and 8mer meiRNA. The interacting portion of meiRNA (5′-$U^3U^4C^5$-3′) is on the hydrophobic and alkaline surface of the β-sheet and the β4–αC loop, with the other portions ($U^6G^7C^8$) of 8mer meiRNA either lying outside Mei2 RRM3 or making few non-specific contacts with the other 8mer meiRNA due to crystal packing (Figure 3B and C). To demonstrate crystal contacts between the 3′ terminal nucleotides ($U^6G^7C^8$) of

Table 1 Data collection and refinement statistics.

	Mei2 RRM3$^{SeMet\text{-}derivative}$	Mei2 RRM3^{native} (PDB ID: 7EIO)	Mei2 RRM3–meiRNA complex (PDB ID: 7EIU)
Wavelength (Å)	0.9785	0.9785	0.9785
Space group	$P4_1$	$P4_1$	$C222_1$
Cell parameters			
a, *b*, *c* (Å)	74.42, 74.42, 67.98	74.55, 74.55, 68.24	66.23, 162.12, 96.66
α, β, γ (°)	90, 90, 90	90, 90, 90	90, 90, 90
Resolution (Å)	40.00–1.90 (1.93–1.90)[a]	40.00–1.90 (1.93–1.90)[a]	40–2.35 (2.39–2.35)[a]
R_{merge} (%)	10.6 (100.6)	7.4 (100.2)	11.9 (81.0)
$I/\sigma I$	54.57 (4.40)	35.76 (2.57)	18.15 (2.91)
Completeness (%)	99.7 (99.9)	99.9 (100)	99.9 (99.9)
$CC_{1/2}$	99.6 (98.5)	100 (72.6)	99.4 (80.3)
Average redundancy	13.6 (13.5)	13.1 (10.8)	7.3 (7.5)
Number of Se site	8/8	/	/
Overall FOM	0.55	/	/
Refinement			
Number of reflections (overall)	/	29356	21980
Number of reflections (test set)	/	1532	1059
R_{work}/R_{free} (%)	/	18.94/22.53	18.34/22.61
Number of atoms			
Mei2 RRM3	/	2353	2364
meiRNA	/	/	246
H_2O	/	181	91
B factors (Å^2)			
Mei2 RRM3	/	29.20	35.58
meiRNA	/	/	35.28
H_2O	/	27.63	36.48
rmsd			
Bond lengths (Å)	/	0.007	0.0024
Bond angles (°)	/	0.762	0.612
Rampage plot % residues			
Favored	/	99.31	98.98
Allowed	/	0.69	1.02
Outliers	/	0	0

[a] Values in parentheses are for the highest-resolution shell.

two RNA molecules due to crystal packing, we performed size-exclusion chromatography multi-angle light scattering (SEC–MALS) experiments, which indicated that Mei2 RRM3 interacts with 8mer meiRNA in a 1:1 stoichiometry (Supplementary Figure S4A).

Molecular details of Mei2 RRM3 in complex with 8mer meiRNA

The $U^3U^4C^5$ segment of 8mer meiRNA is positioned over the four-stranded β-sheet surface in the Mei2 RRM3–RNA complex. Key inter-molecular contributions conserve aromatic amino acids projecting from the RNA-binding surface of the RRM domain. Mei2 RRM3 interacts specifically with the U^3U^4 dinucleotide sequence via a 'nucleobase pocket' formed by the β-sheet surface and the β4–αC loop (Figure 4A and B). The nucleobase pocket's stereochemical and electrostatic features result in several stabilizing interactions with RNA. Although the C^5 base is outside the pocket, it interacts with αC residues (Figure 4A and B). At the first nucleobase position, the U^3 nucleotide is located in a small pocket formed by the residues of the β4–αC loop and donates many hydrogen bonds. The side chain of S677 forms a hydrogen bond with the carbonyl of the U^3 base. The N5 of the U^3 base forms a hydrogen bond with the main chain of Y678. The NH_2 atoms of N582 donate a hydrogen bond to the carbonyl of the U^3 base. The side chain of N680 forms a hydrogen bond with the ribose sugar rings of U^3, and the backbone amide of N680 forms a hydrogen bond with the U^3 base (Figure 5A). At the second nucleobase position, the U^4 of meiRNA is in a hydrophobic pocket formed by the side chain of F644 and I681 of Mei2 RRM3. F644 π–π stacks below the base of U^4. Such a protein-based stacking triad seems to play an indispensable role in the Mei2 RRM3–meiRNA interaction since Mei2 RRM3^{F644A} is impaired significantly in binding to wild-type meiRNA. The U^4 base also makes two hydrogen bonds with the backbone amides of N680 and I681, respectively (Figure 5B). At the third nucleobase position, although C^5 is outside the pocket, this nucleotide is recognized specifically. The ζ-amino group of K690 from αC donates two hydrogen bonds to the carbonyl oxygen of the C^5 nucleotide. The side chains of R631 and Y629 interact with the phosphate group of C^5 (Figure 5C).

To determine whether these key residues of Mei2 RRM3 are required for binding with meiRNA *in vitro*, we introduced alanine and glutamate mutations into Mei2 RRM3. Subsequently, we performed FP assays to measure the binding affinities of different Mei2 RRM3 mutants with 8mer meiRNA. Mutation of the F644 residue, which is involved in stacking interactions with the

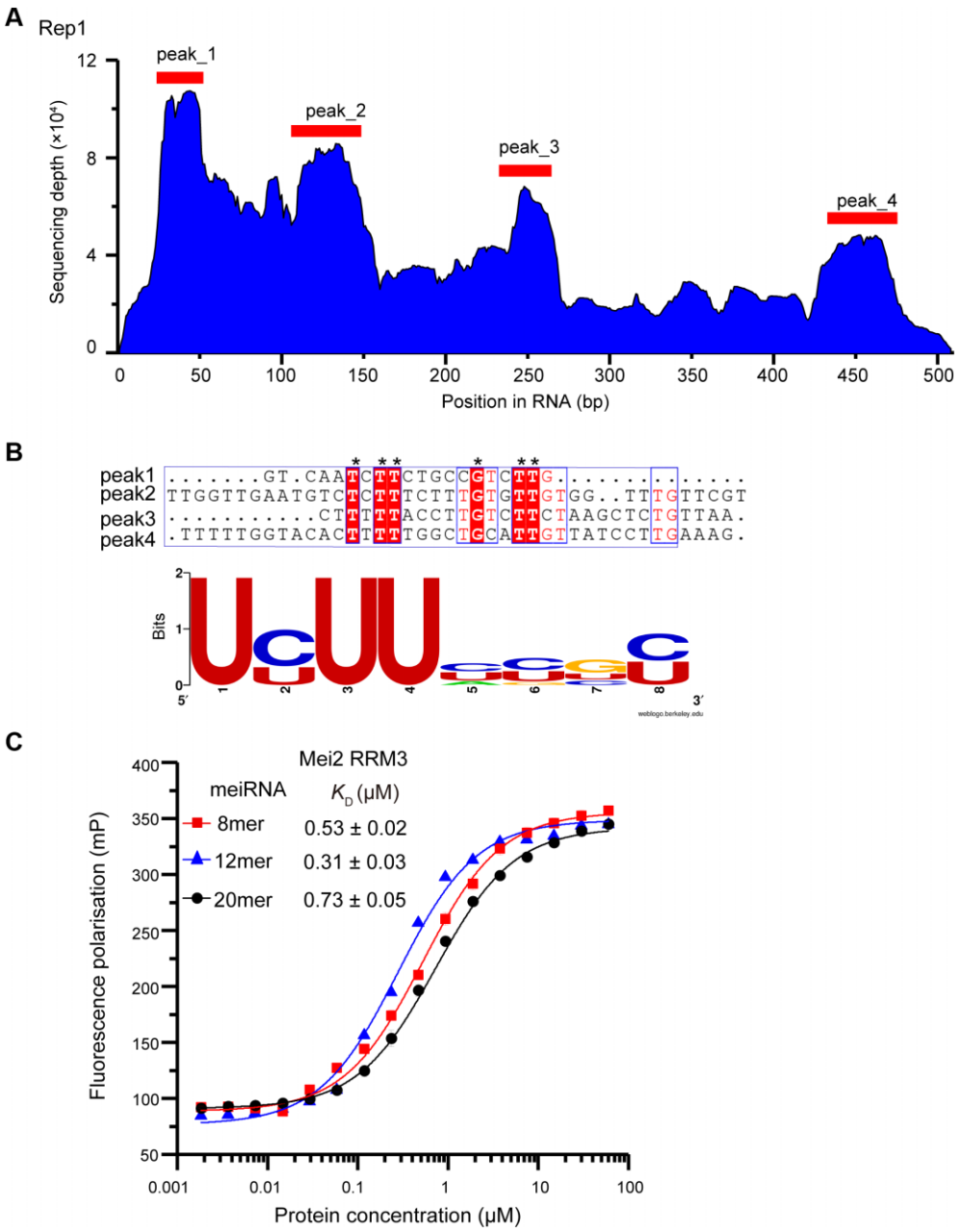

Figure 2 Mei2 RRM3 prefers to recognize U-rich RNA sequences. (**A**) RNA fragments interacting with Mei2 RRM3 were mapped to the meiRNA sequence using Bowtie2. (**B**) Sequence alignments of four peaks of *in vitro* CLIP–seq. Conserved RNA motifs of meiRNA are in red frames (red squares, identical nucleotides; black star, conserved RNA motif involved in Mei2 RRM3 interaction). Consensus motifs were identified by *in vitro* CLIP–seq and WebLogo analysis of the four RNA-binding sites. (**C**) Fluorescence polarization fitting curves of Mei2 RRM3^{WT} using 8mer meiRNA (UUCUCUGC, red), 12mer meiRNA (UCAAUCUUCUGC, blue), and 20mer meiRNA (GUCAAUCUUCUGCCGUCUUG, black).

U^4 bases in the complex, resulted in a severe affinity reduction to 8mer meiRNA. A double mutant (F644/I681), which formed a U^4-binding pocket, resulted in undetectable binding (Figure 4C; Supplementary Table S3). Therefore, recognition of the U^4 nucleotide seems to play an indispensable role in the Mei2 RRM3–8mer meiRNA interaction. Ala mutations of N680 and K690, or reverse charge mutation of R631 to Asp, also reduced the affinity to 8mer meiRNA (Figure 4C; Supplementary Table S3).

The UUC(U) motif of meiRNA is recognized specifically by Mei2 RRM3

Previous *in vitro* CLIP–seq experiments have revealed that Mei2 RRM3 preferred U-rich motifs. We performed FP assays by titrating Mei2 RRM3 against carboxyfluorescein (FAM)-labelled 8mer meiRNA and its mutants to confirm the sequence-specific preference of Mei2 RRM3. Mutation of the uracil base of U^3 to guanine ($U^1C^2\underline{G}^3U^4C^5U^6G^7C^8$), adenine ($U^1C^2\underline{A}^3U^4C^5U^6G^7C^8$),

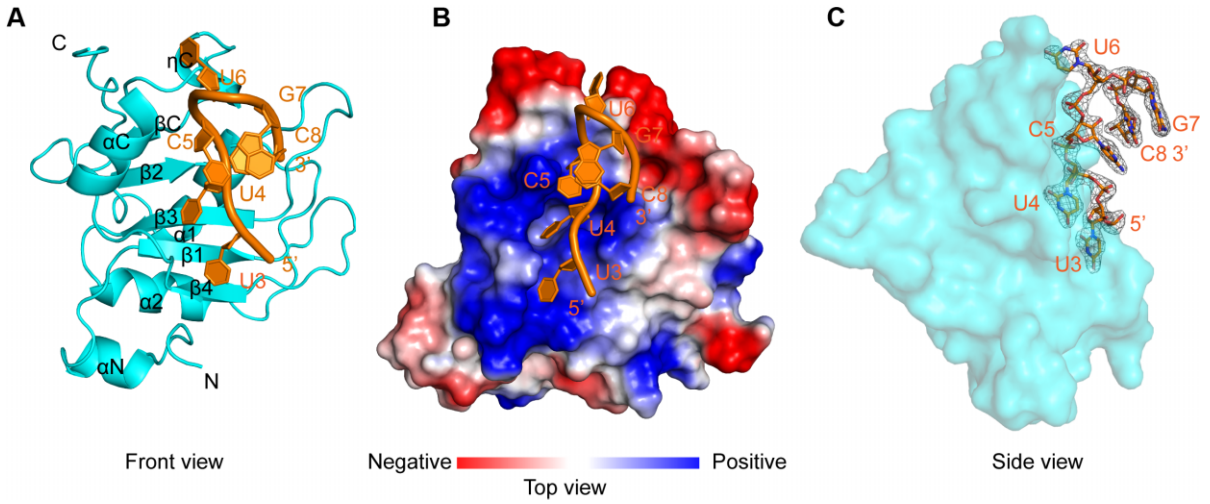

Figure 3 The structure of Mei2 RRM3 in complex with meiRNA. (**A**) Ribbon representation of Mei2 RRM3 bound to 8mer meiRNA (front view). Mei2 RRM3 is colored in cyan. The bound 8mer meiRNA is colored in orange. (**B**) Electrostatic surface potential map of Mei2 RRM3 in complex with 8mer meiRNA (top view). Red and blue colors denote negative and positive surface charges, respectively. (**C**) The Van der Waals surface view of Mei2 RRM3 interaction with 8mer meiRNA. The Van der Waals surface of Mei2 RRM3 is depicted as a semitransparent surface (cyan). 8mer meiRNA (orange) is shown as sticks. The *2Fo-Fc* electron density (gray mesh) for 8mer meiRNA contoured at 1.5σ is shown.

or cytosine ($U^1C^2\underline{C}^3U^4C^5U^6G^7C^8$) reduced the affinity by a factor of three to six (K_D values of 3.11 ± 0.44 μM, 1.82 ± 0.27 μM, and 1.55 ± 0.17 μM, respectively, as compared to a K_D of 0.53 ± 0.02 μM for the ligand with uracil; Figure 5D; Supplementary Table S3). Furthermore, mutation of the uracil base of U^4 to guanine ($U^1C^2U^3\underline{G}^4C^5U^6G^7C^8$), adenine ($U^1C^2U^3\underline{A}^4C^5U^6G^7C^8$), or cytosine ($U^1C^2U^3\underline{C}^4C^5U^6G^7C^8$) reduced the affinity by a factor of three to five (K_D values of 3.05 ± 0.32 μM, 1.72 ± 0.17 μM, and 1.35 ± 0.11 μM, respectively; Figure 5E; Supplementary Table S3). Mutation of the cytosine base of C^5 to guanine ($U^1C^2U^3U^4\underline{G}^5U^6G^7C^8$) or adenine ($U^1C^2U^3U^4\underline{A}^5U^6G^7C^8$) reduced the affinity by a factor of three to eight (K_D values of 1.45 ± 0.14 μM and 4.12 ± 0.18 μM, respectively; Figure 5F; Supplementary Table S3). However, mutation of the base of C^5 to uracil ($U^1C^2U^3U^4\underline{U}^5U^6G^7C^8$) did not significantly alter the binding of Mei2 RRM3 (K_D values of 0.37 ± 0.03 μM; Figure 5F; Supplementary Table S3). Compared with the mutation to adenine or cytosine, the mutation of all three nucleotides of 8mer meiRNA to guanine affected the affinity more significantly. Based on the results of single point mutations, we designed multi-mutations of 8mer meiRNA. We found that Mei2 RRM3 preferred binding to U-rich motifs, consistent with previous *in vitro* CLIP–seq experimental results, since both dual-mutants (meiRNA^{mut1}, $U^1C^2\underline{G}^3\underline{G}^4C^5U^6G^7C^8$) and poly-G (meiRNA^{mut2}, $\underline{G}^1\underline{G}^2\underline{G}^3\underline{G}^4\underline{G}^5\underline{G}^6\underline{G}^7\underline{G}^8$) are significantly impaired in binding to wild-type Mei2 RRM3 (Figure 5G; Supplementary Table S3). These results indicate that sequence-specific interactions are important for the binding affinity of Mei2 RRM3 with meiRNA. Previous *in vitro* CLIP–seq experiments have found that Mei2 RRM3 preferred binding to U-rich RNA fragments. The molecular details of the Mei2–meiRNA complex and the mutation experiments indicated that Mei2 RRM specifically interacted with the UUC(U) motif of meiRNA. These data indicate that the RNA-binding preference of Mei2 RRM3 is the UUC(U) motif of meiRNA.

Structure-based Mei2 mutations cause defective karyogamy

We then tested the effect of the Mei2 mutation on meiosis in fission yeast cells. We expressed full-length Mei2^{WT}-Myc and the Mei2 mutant Mei2^{F644A}-Myc from a Mei2 promoter in *mei2*Δ cells and took microscopic images 10.5 h after two mating types of cells were crossed on sporulation medium. As shown in Figure 6A and B, more zygotes were found in wild-type cells and the *mei2*Δ cells expressing full-length Mei2^{WT}-Myc than that in *mei2*Δ cells or the *mei2*Δ cells expressing Mei2^{F644A}-Myc. We further examined cells expressing Cnp1-GFP (an inner kinetochore protein) and mCherry-Atb2 (α-tubulin) by microscopy 10.5 h after two mating types of cells were mixed and cultured on sporulation medium. Hoechst was used to stain the nucleus. Many of the *mei2*Δ zygotes (95.9%) and the *mei2*Δ zygotes expressing Mei2^{F644A}-Myc (92.5%) displayed separated nuclei, probably due to defective karyogamy (Figure 6C and D). In contrast, only 23.1% of wild-type cells and 49.3% of *mei2*Δ zygotes expressing Mei2^{WT}-Myc had separated nuclei (Figure 6C and D; Supplementary Figure S5A and S5B). We then employed quantitative polymerase chain reaction (qPCR) to test the expression levels of the meiosis-specific transcripts *mei4* and *ssm4*. The expression levels of both *mei4* and *ssm4* mRNAs decreased significantly in *mei2*Δ cells and the *mei2*Δ cells expressing Mei2^{F644A} mutant, but not in the *mei2*Δ cells expressing Mei2^{WT} (Figure 6E; Supplementary Figure S5C). Consistent with previous results (Harigaya and Yamamoto, 2007), we found that the residue F644 of Mei2 is important for the interaction between

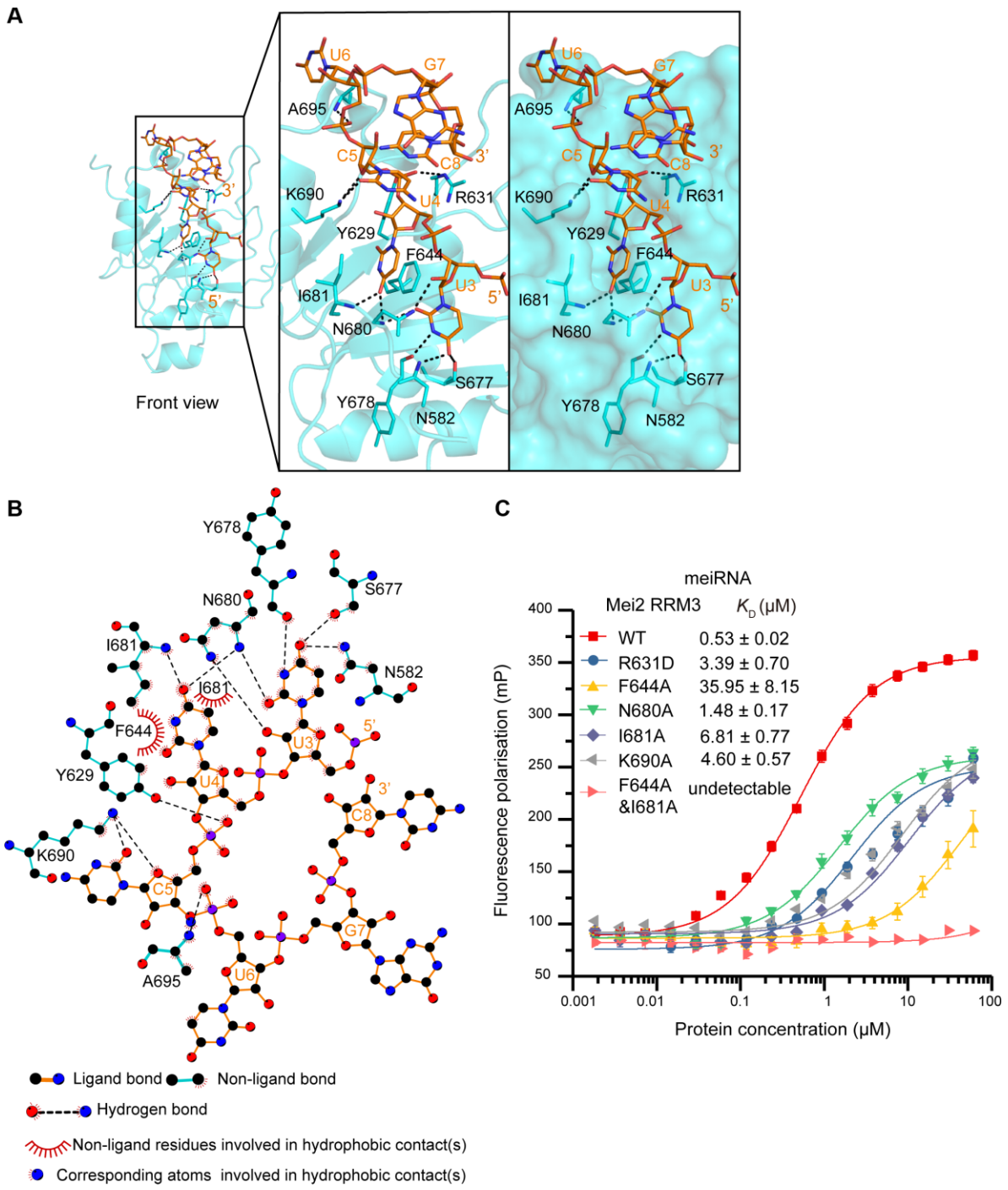

Figure 4 Molecular interface between Mei2 RRM3 and meiRNA. (**A**) Close-up views of the interactions between Mei2 RRM3 and 8mer meiRNA. Left: Mei2 RRM3 (cyan) is shown as ribbons with the selected side chain as sticks. 8mer meiRNA (orange) is shown as sticks. Hydrogen bonds are shown as black dashed lines. Right: Van der Waals surface view of Mei2 RRM3 interaction with 8mer meiRNA. The Van der Waals surface of Mei2 RRM3 is depicted as a semitransparent surface (cyan). 8mer meiRNA is represented as sticks (orange). (**B**) Interaction plot between Mei2 RRM3 and 8mer meiRNA (plot produced using LigPlot^{+} v. 1.4). (**C**) Fluorescence polarization fitting curves of 8mer meiRNA^{WT} using Mei2 RRM3^{WT} (red), Mei2 RRM3 ^{R631D} (blue), Mei2 RRM3^{F644A} (yellow), Mei2 RRM3^{N680A} (green), Mei2 RRM3 ^{I681A}(slate), Mei2 RRM3^{K690A} (gray), and Mei2 RRM3$^{F644A/I681A}$ (pink).

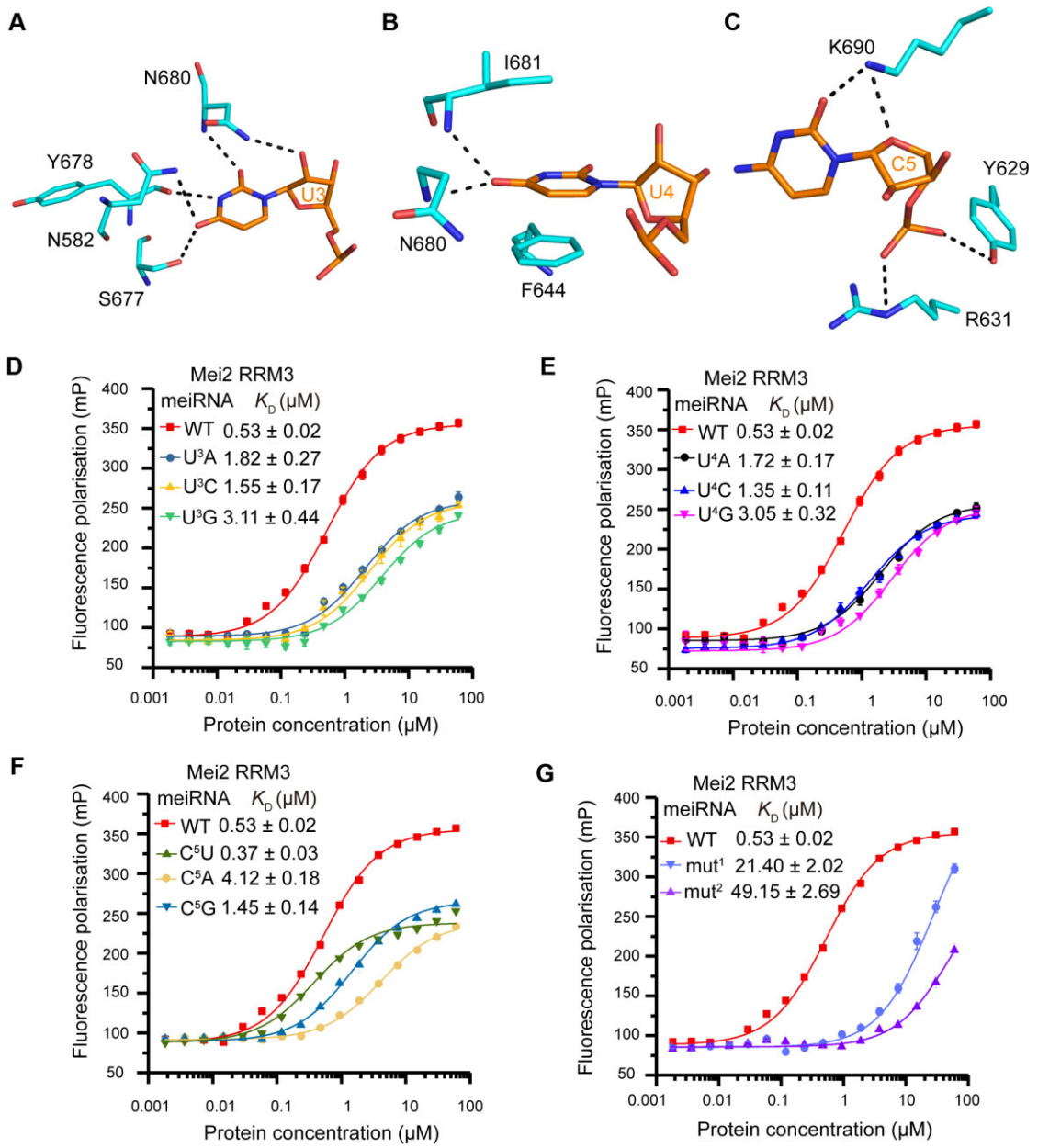

Figure 5 UUC(U) motif is recognized specifically by Mei2 RRM3. (**A**–**C**) Detailed base-specific interactions between Mei2 RRM3 key residues (cyan) and 'U^3-U^4-C^5' of 8mer meiRNA (orange). The hydrogen-bonding interactions are depicted as black dashed lines. (**D**) Fluorescence polarization fitting curves of 8mer meiRNA^{WT} (UCUUCUGC, red), U^3A (UCAUCUGC, blue), U^3C (UCCUCUGC, yellow), and U^3G (UCGUCUGC, green) using Mei2 RRM3^{WT}. (**E**) Fluorescence polarization fitting curves of 8mer meiRNA^{WT} (UCUUCUGC, red), U^4A (UCUACUGC, black), U^4C (UCUCCUGC, deep blue), and U^4G (UCUGCUGC, magentas) using Mei2 RRM3^{WT}. (**F**) Fluorescence polarization fitting curves of 8mer meiRNA^{WT} (UCUUCUGC, red), C^5U (UCUUUUGC, smudge), C^5A (UCUUAUGC, light orange), and C^5G (UCUUGUGC, deep teal) using Mei2 RRM3^{WT}. (**G**) Fluorescence polarization fitting curves of 8mer meiRNA^{WT} (UCUUCUGC, red), 8mer meiRNA^{mut1} (UCGGCUGC, light blue), and 8mer meiRNA^{mut2} (GGGGGGGG, slate) using Mei2 RRM3^{WT}.

Mei2 and meiRNA. Therefore, the results also indicate that the RNA-binding ability of Mei2 plays a crucial role in meiosis.

Microscopic analysis was then performed to examine meiotic wild-type and *sme2*Δ (obtained from the Yeast Genetic Resource Center at Osaka City University) cells. Specifically, images were taken at 10.5 h after two mating types of cells were mixed on sporulation medium. Results showed no significant difference of the percentage of zygotic cells between *sme2*Δ cells (7.4%) and wild-type cells (8.0%). In addition, 90% of wild-type zygotic cells displayed fused nuclei, and 89% of *sme2*Δ zygotic cells displayed fused nuclei, indicative of a functional karyogamy process in *sme2*Δ cells (Supplementary Figure S6A–C). Therefore,

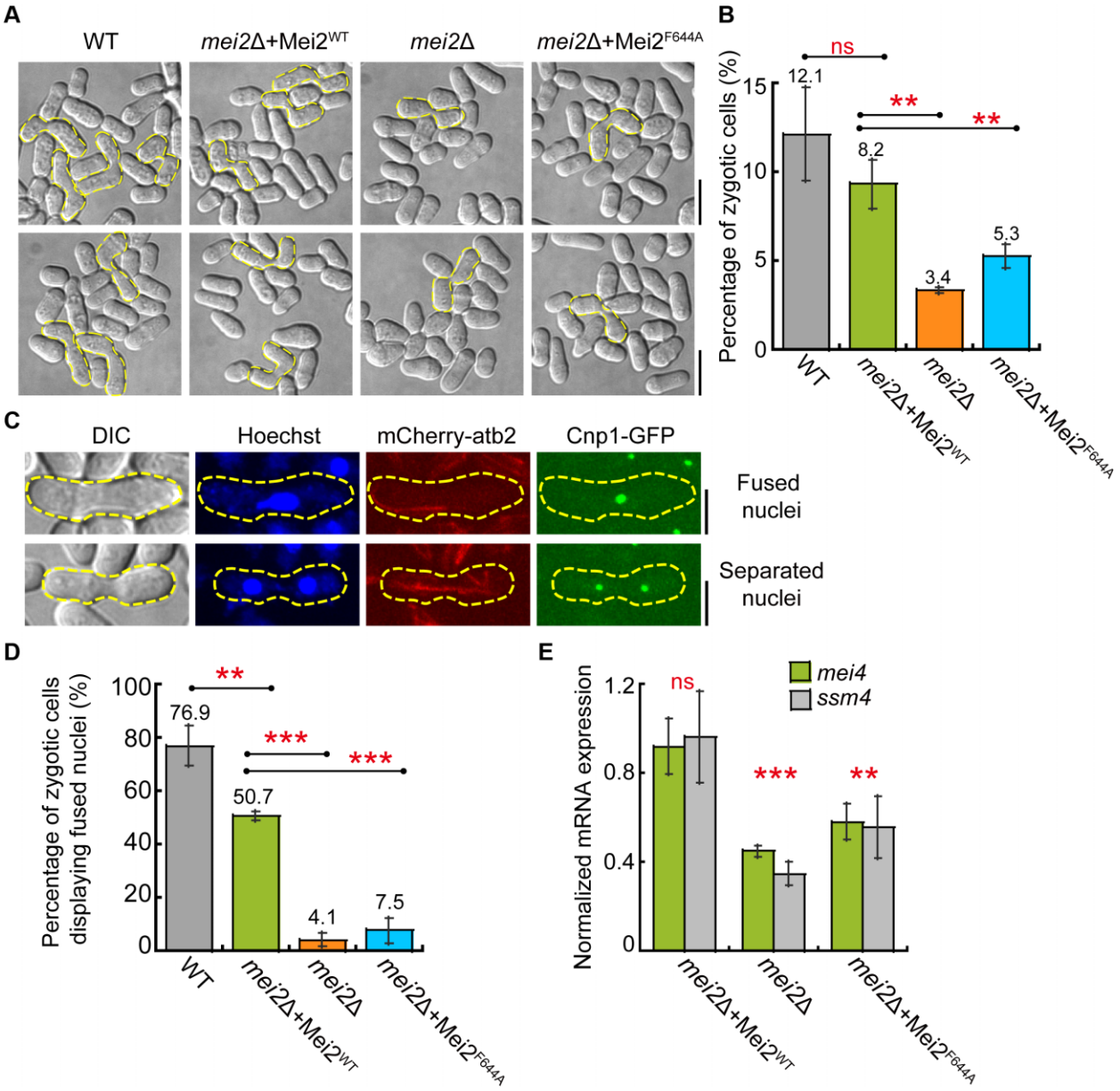

Figure 6 Structure-based Mei2 mutation causes defective karyogamy. (**A**) Bright-field images of wild-type (WT), *mei2*Δ cells, and *mei2*Δ cells ectopically expressing full-length Mei2 or Mei2^{F644A}. Images were taken at 10.5 h after two mating types of cells were mixed on sporulation medium. Yellow dashed lines mark zygotic cells. Scale bar, 10 μm. (**B**) Quantification of the percentage of zygotic cells indicated in **A**. The experiments were repeated three times ($n = 3$). Error bars represent SD, and cell number analyzed was >536. Statistics were calculated by the Kaleida Graph (ns, $P = 0.20$; $^{**}P < 0.05$; $^{***}P < 0.005$). (**C**) Maximum projection images of zygotic cells displaying fused or separated nuclei. Hoechst staining marks the nucleus, and yellow dashed lines mark the outline of cells. Images were taken at 10.5 h after two mating types of cells were mixed on sporulation medium. Scale bar, 5 μm. DIC, differential interference contrast. (**D**) Quantification of the percentage of zygotic cells displaying fused nuclei in **C**. The experiments were repeated three times ($n = 3$). Error bars represent SD, and cell number analyzed was >49. Statistics were calculated by the Kaleida Graph ($^{**}P < 0.05$; $^{***}P < 0.005$). (**E**) mRNA expression levels of *ssm4* and *mei4* in *mei2*Δ alone or expressing Mei2^{WT} or Mei2^{F644A} were determined by qPCR and normalized against that in WT cells. The experiments were repeated three times. Error bars represent SD and statistics were calculated by the Kaleida Graph (ns, $P = 0.34$; $^{**}P < 0.05$; $^{***}P < 0.005$).

karyogamy may not be impaired in *sme2*Δ cells. To determine the function of meiRNA *in vivo*, we further checked the formation of spores after two mating types of cells were mixed on malt extract (ME) plates for 24 h. The results showed that *sme2*Δ zygotes did not form spores, although they appeared to undergo normal karyogamy (Supplementary Figure S6D). Taken together, meiRNA is essential for spore formation but is not required for karyogamy.

The multiple interactions between Mei2, meiRNA, Erh1, and Mmi1 in Mei2 dot

Previous studies have reported that deletion of the two amino-terminal RRMs does not impair the function of Mei2 significantly (Watanabe et al., 1997). In contrast, the removal of Mei2 RRM3 inactivated its function completely. A Mei2 derivative consisting of residues 429–733, containing only the Mei2 RRM3, was the shortest construct to be functional *in vivo*. In addition, a GST fusion protein carrying Mei2 RRM3 (residues 429–750) could bind to meiRNA *in vitro*, as did another carrying residues 30–750 (Watanabe et al., 1997). Therefore, we employed an *in vitro* CLIP–seq assay to map the binding region of meiRNA by Mei2 RRM3 directly. To further prove this point, the GST-tagged Mei2 RRM1-RRM2 (residues 191–373) was purified. We evaluated the meiRNA-binding potential of Mei2 RRM1-RRM2 (residues 191–373) by performing EMSA experiments with 5′-FAM-20mer meiRNA (5′-FAM-GUCAAUCUUCUGCCGUCUUG-3′), which is the meiRNA fragment of the CLIP–seq-identified peak_1. Mei2 RRM1-RRM2 was unable to shift the 5′-FAM-20mer meiRNA (Figure 7A and B). Next, we purified the MBP-tagged Mei2 RRM2-(Gly-Ser-Ser)$_5$-RRM3 and measured its binding affinity with 5′-FAM-20mer meiRNA by FP binding assay. The K_D value of MBP-tagged Mei2 RRM2-(Gly-Ser-Ser)$_5$-RRM3 to 20mer meiRNA is 0.54 ± 0.03 μM, which is very similar to that of Mei2 RRM3 (0.73 ± 0.05 μM) (Figure 7A and C). Consistent with previous results, Mei2 RRM1-RRM2 plays a dispensable role in the Mei2–meiRNA interaction, and Mei2 RRM3 is necessary and sufficient for Mei2 to interact with meiRNA. Hence, the result that Mei2 RRM1-RRM2 does not bind to meiRNA may suggest that Mei2 RRM1-RRM2 could be forming a contact with another RNA-binding partner or instead mediating a protein–protein interaction.

Although Mei2 contains three RRMs, Mei2 RRM3 is essential for Mei2 to interact with meiRNA. There is a question whether Mei2 can distinguish its target meiRNA only using Mei2 RRM3. According to previous studies (Harigaya et al., 2006; Sugiyama et al., 2016) and our experimental data, we rationalize that Mei2 distinguishes its target meiRNA through multi-interactions among Mei2, meiRNA, Erh1, and Mmi1. Mei2 dot mainly contains four components Mei2, meiRNA, Erh1, and Mmi1 according to recent research (Harigaya et al., 2006; Sugiyama et al., 2016). Mmi1 interacts with the 3′ region of meiRNA, which carries ample DSR motifs (UNAAAC), whereas Mei2 interacts preferentially with the 5′ region of meiRNA (Yamashita et al., 2012; Wang et al., 2016). Erh1 and Mmi1 form a tight complex, which was termed the Erh1–Mmi1 complex (EMC) (Sugiyama et al., 2016; Xie et al., 2019). Our group has identified that Erh1 interacts with the amino-terminal domain of Mmi1 (the Erh1-interacting domain) and determined the co-crystal structure of the EMC that consists of Erh1 homodimers interacting with Mmi1 in a 2:2 stoichiometry via a conserved molecular interface (Xie et al., 2019). During meiosis, Erh1 co-localizes with the Mei2–meiRNA dot and is required for its formation. The lack of Mei2 dot in *erh1*Δ indicates that Erh1 facilitates proper Mei2 localization (Sugiyama et al., 2016). To investigate whether Mei2 interacts with Erh1 directly, we have purified GST-tagged Mei2$^{429–750}$ and Mei2$^{571–750}$. We found that the purified GST-tagged Mei2$^{429–750}$ bound efficiently to Erh1 (Figure 7D). These results show that Mei2 interacts with Erh1 directly *in vivo* and *in vitro*. Taken together, the multiple interactions among Mei2 meiRNA, Erh1, and Mmi1 confer the specific recognition of meiRNA and the formation of Mei2 dot (Figure 7E).

Discussion

Mei2 is required for initiating premeiotic DNA synthesis and meiosis in fission yeast. The conserved C-terminal RRM of Mei2 plays an essential role in recognizing meiRNA and is required for meiosis initiation. In our study, we determined the structure of Mei2 RRM3 using a natural 8mer meiRNA fragment identified by *in vitro* CLIP–seq. We found that the specific recognition of meiRNA by Mei2 RRM3 is indispensable for the meiosis process. We also identified the binding preference of Mei2 RRM3 for the UUC(U) motif *in vitro*.

We showed that the Mei2 RRM3 structures are very similar in the RNA-free and RNA-bound states, with differences observed in the loop joining α2 and β4, which is not involved in protein–RNA interactions in the complex. Compared to the RNA-free state, a ‘nucleotide pocket’ was induced on the electrostatic surface in RNA-bound states due to the binding of 8mer meiRNA (Supplementary Figure S7A and B). F644 is conformationally changed because the residue F644 forms π–π stacking below the base of U^4 (Supplementary Figure S7C). The complex is stabilized by inter-molecular staking interactions, as observed between U4 and F644. Thus, mutation of F644 leads to significant impairment of binding to meiRNA (Figure 4C). Similarly, mutational disruption of the U4-binding pocket (dual F644A/I681A mutation) resulted in a complete loss of binding affinity.

The structure of Mei2 RRM in complex with 8mer meiRNA demonstrates a unique mode of RNA recognition by the RRM domain and contains several typical attributes (Clery et al., 2008). However, some features are unique to the mode of recognition of Mei2 RRM3. These features include the binding of U^3 and C^5. The U^3 nucleotide is located in a nucleotide pocket formed by the residues of the β4–αC loop and donates multiple hydrogen bonds that are important for sequence specificity. Although previous studies have reported the crucial role of loops in RRM for RNA binding, these investigations just involved loops β1/α1, β2/β3, and α2/β4 (Auweter et al., 2006; Dominguez and Allain, 2006; Skrisovska et al., 2007). Also, Mei2 RRM3 contributes to the interaction with the nucleotide C^5 using the key residue K690 in αC, but not via the canonical β-sheet binding interface, with the main RNA-binding site in the C-terminal domain.

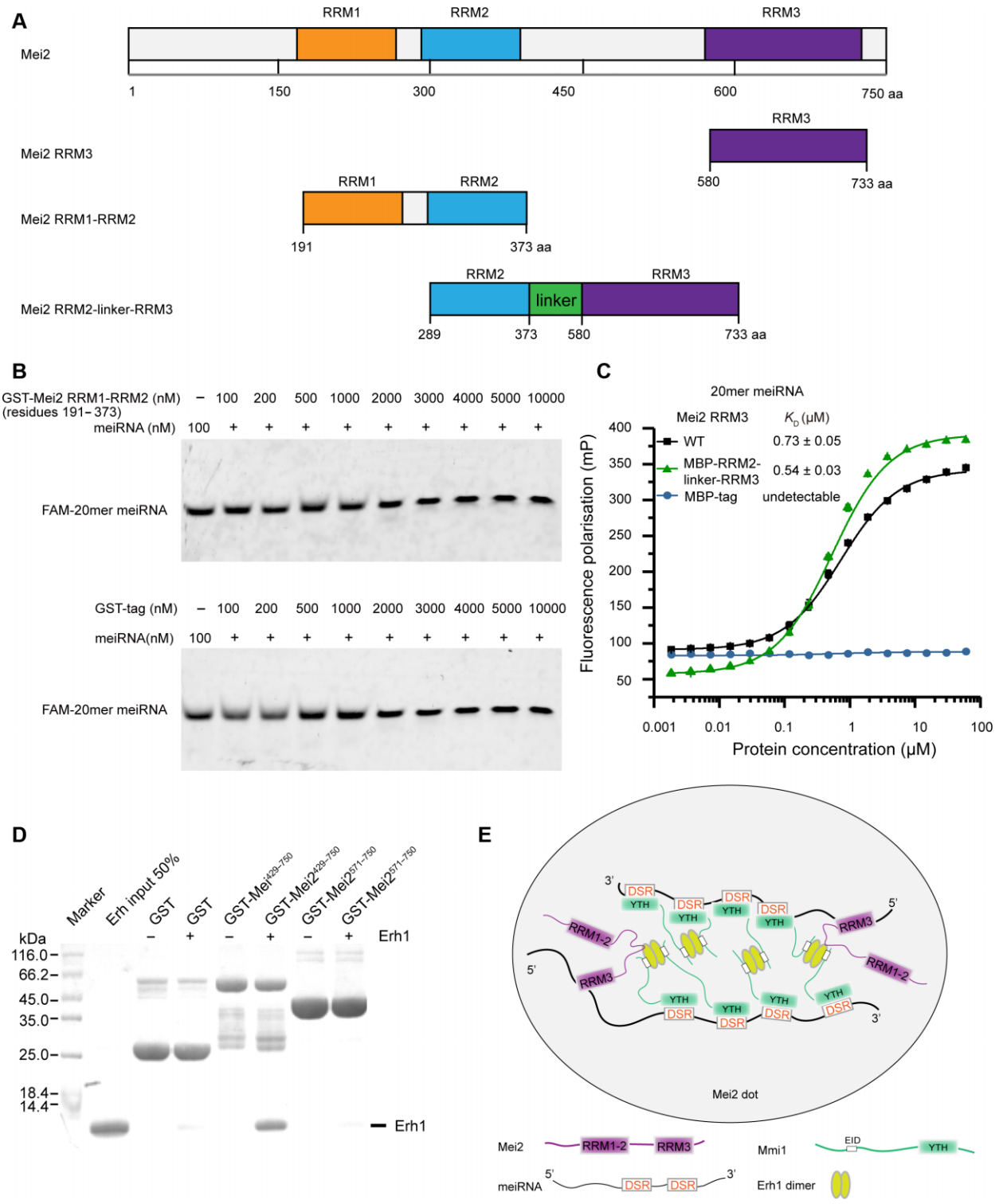

Figure 7 The multiple interactions between Mei2, meiRNA, Erh1, and Mmi1 in Mei2 dot. (**A**) Domain organization of the *S. pombe* Mei2 protein. (**B**) EMSA experiments with 5′-FAM-20mer meiRNA and GST-Mei2 RRM1-RRM2. (**C**) Fluorescence polarization fitting curves of Mei2 RRM3 (black), MBP fusion Mei2 RRM2-(Gly-Ser-Ser)$_5$-RRM3 (green), and MBP tag (blue) using 20mer meiRNA (5′-FAM-GUCAAUCUUCUGCCGUCUUG-3′). (**D**) Interactions of GST-tagged Mei2 protein with Erh1 visualized by Coomassie blue staining. The indicated GST-Mei2 fusion proteins or GST alone were incubated with Erh1. The complexes were collected with glutathione–agarose resin, and the bound proteins were eluted and then subjected to SDS–PAGE. GST or GST-Mei2 fusion proteins without Erh1 are shown as a negative control. (**E**) Model showing interactions of the four components (Mei2, meiRNA, Mmi1, and Erh1) in Mei2 dot.

During the preparation of our manuscript, Mathieu Rougemaille's group presented another Mei2 RRM3–RNA complex structure (PDB ID: 6YYM) (Andric et al., 2021). Unlike our 8mer RNA fragment that is derived from the natural meiRNA sequence by *in vitro* CLIP–seq, they used a 12mer uridine-rich RNA fragment derived from the recognition motif of $RRM1^{5xl}$ (Hennig et al., 2014), which displayed high sequence similarity with Mei2 RRM3 (Supplementary Figure S8A). A super-imposition of these two Mei2 RRM3–RNA structures shows that their overall structures are similar with a rmsd of 0.423 Å for all aligned Cα atoms (Supplementary Figure S8B). Furthermore, both structures specifically recognize a nucleotide triplet. Their recognition modes for the first two nucleotides (U^3U^4 dinucleotide) by Mei2 RRM3 are completely same but show a difference in the recognition of the third nucleotide in the triplet (Supplementary Figure S8C and D). The G^8 nucleotide of RNA^{6YYM} forms π–π stacking interaction with the residue F634; however, in our structure, the base of the C^5 nucleotide of 8mer meiRNA points to an opposite direction and forms two hydrogen bonds with K690 of Mei2 RRM3 (Supplementary Figure S8D). Although in the Mei2 $RRM3^{6YYM}$ structure, the G8 nucleotide further forms intensive interactions with C11 and C12 nucleotides, a deletion of $U^9U^{10}C^{11}C^{12}$ showed similar binding affinity compared to 12mer RNA^{6YYM} (Supplementary Figure S8E), further indicating that the 'UUN' nucleotide triplet plays the dominant role in the recognition. We further tried to mutate F634 to an alanine, but the mutant was expressed as inclusion bodies in *Escherichia coli*. As mentioned before, the Mei2 $RRM3^{K690A}$ mutant showed decreased binding to 8mer RNA. Thus, Mei2 RRM3 may employ a different strategy to recognize the third nucleotide, but this requires further investigation. Nevertheless, according to our FP assays, we showed that Mei2 RRM3 prefers U/C in the third position.

Karyogamy is a step in fusing two nuclei of haploid cells (Gibeaux and Knop, 2013; Merlini et al., 2013). The finding that *mei2* mutants fail to complete nuclear fusion indicates that *mei2* mutants could arrest meiotic initiation, even before Mei2 dot formation. Although meiRNA is a central component of Mei2 dot, our results suggest that meiRNA plays an important role in spore formation rather than karyogamy, which is consistent with previous findings that meiRNA is essential for meiosis I and Mei2 dot formation (Watanabe and Yamamoto, 1994; Harigaya et al., 2006). These results indicate that Mei2 binds to different partners to perform different functions during meiosis (Yamashita et al., 1998; Shichino et al., 2014; Mukherjee et al., 2018). However, the RNA partners that bind to Mei2 and cooperate with Mei2 to regulate karyogamy have not been identified. The RNA-binding motif we identified in the study paves the way for the identification of other partners that can interact with Mei2. The mitosis–meiosis switch requires further investigation to increase our understanding of this process that is fundamental in many organisms. AML is the *Arabidopsis* homolog of Mei2 and contains a domain similar to Mei2 RRM3 (Kaur et al., 2006). The control of meiosis in plants involves integrating nutrition-dependent signaling pathways and is similar to the situation in fission yeast. Hence, our studies may provide insights into the role of AML in plant meiosis.

Materials and methods

Protein and RNA generations

The full-length *S. pombe mei2* gene was cloned in the pET28a vector (TransGen Biotech co. Ltd). The DNA sequences of Mei2 RRM3 (residues 580–733) and Erh1 were amplified and cloned into a modified pET28a plasmid (Novagen), which contained an N-terminal 6×His-tag and a TEV protease cleavage site. The DNA sequences of Mei2 RRM1-RRM2 (residues 191–373), $Mei2^{571–750}$ (residues 571–750), and $Mei2^{580–733}$ (residues 580–733) were amplified and cloned into a modified pGEX4T-1 plasmid (Novagen), which contained an N-terminal GST-tag and a TEV protease cleavage site. The DNA sequence of Mei2 RRM2-linker-RRM3 (residue 289–373 linker 580–733) was amplified and cloned into a modified pET22b plasmid (Novagen), which contained an N-terminal MBP-tag and a TEV protease cleavage site. The mutants were generated using a MutanBEST kit (TaKaRa Bio Inc.) and verified by DNA sequencing.

Proteins were overexpressed in *E. coli* BL21(DE3) cells (Novagen) cultured in Luria–Bertani (LB) medium containing kanamycin (50 μg/ml). Cells were grown in LB medium at 37°C until the OD_{600} reached ∼0.8. Protein expression was induced with 0.3 mM β-D-1-thiogalactopyranosid for 24 h at 16°C. Cells were harvested by centrifugation, and cell pellets from 1 L of culture were resuspended in 50 ml of pre-cooled buffer A (20 mM Bis–Tris–HCl, pH 6.5, and 1 M NaCl) and lysed by sonication on ice. The protein-containing supernatant was subjected to affinity chromatography using a Ni^{2+}-chelating column (GE Healthcare) and eluted with pre-cooled buffer B (20 mM Bis–Tris–HCl, pH 6.5, 1 M NaCl, and 0.5 M imidazole). The purified fusion protein was digested overnight at 16°C with 6×His-tagged TEV protease and dialyzed to buffer C (20 mM Bis–Tris–HCl, pH 6.5, and 150 mM NaCl). The cleaved 6×His-tag and residual TEV protease were removed using a Ni^{2+}-chelating column. The proteins were purified further by SEC on a Hiload 16/60 Superdex 75 column (GE Healthcare) in buffer C (20 mM Bis–Tris–HCl, pH 6.5, and 150 mM NaCl).

RNA oligomers were purchased from TaKaRa Bio Inc. and dissolved in diethylpyrocarbonate (DEPC)-treated water to a final concentration of 10 mM. RNA oligomers used in this study are listed in Supplementary Table S1.

Protein crystallization, data collection, and structure determination

Crystallization was performed by the hanging drop vapor diffusion method at 20°C by mixing 0.1 μl protein solution with 0.1 μl reservoir solution for the primary screening. The volume of protein and reservoir solution was adjusted to 1 μl during optimization. Native and SeMet-derivative apoMei2 RRM3 proteins (15 mg/ml) were crystallized in a reservoir solution containing 0.49 M sodium phosphate monobasic monohydrate and 0.91 M potassium phosphate dibasic, pH 6.9. The crystals of native Mei2 RRM3 with an 8mer meiRNA complex (1:1.5 molar

ratio, 10 mg/ml) were grown in the condition containing 0.2 M ammonium sulfate, Bis–Tris–HCl, pH 6.5, and 25% PEG3350. Crystals were soaked in the reservoir solution supplemented with 25% (*v*/*v*) glycerol and flash-frozen in liquid nitrogen. X-ray diffraction data were collected using beamline 19U1 of Shanghai Synchrotron Radiation Facility. The data were manipulated using the HKL2000 software (Otwinowski and Minor, 1997). Single-wavelength anomalous scattering data were collected from a crystal of SeMet-derivative apoMei2 RRM3. The initial phase was calculated using AutoSol in PHENIX, and the initial model was built using AutoBuild in PHENIX (Adams et al., 2010). The initial model was then completed through several cycles of manual model rebuilding in Coot and refinement in REFMAC5 (Emsley et al., 2010; Murshudov et al., 2011). The structure of the native apoMei2 RRM3 was determined by molecular replacement with the program MOLREP in CCP4i (Vagin and Teplyakov, 2010). Iterative manual model building and refinement with Phenix.refine produced the current model of the two RRMs in the asymmetric unit (PDB ID: 7EIO). The complex structures were determined by molecular replacement with the MOLREP program using the structure of apoMei2 RRM3 (PDB ID: 7EIO) as the search model (Navaza and Saludjian, 1997; McCoy et al., 2007). The model was further built and refined using Coot and Phenix.refine (Adams et al., 2010). All the structural figures were generated by PyMOL (Schrödinger, https://www.pymol.org/). Table 1 summarizes the data processing statistics.

RNA preparation

The meiRNA (1–508 nt) was used for *in vitro* CLIP–seq experiments. The RNA was transcribed and purified *in vitro* (Lv et al., 2019). The DNA template used to transcribe the meiRNA was synthesized by TaKaRa Bio Inc. and dissolved in DEPC-treated water to a final concentration of 100 mM. The reaction mixture comprised 10 mM Tris, 10 mM DTT, 10 mM NTPs, 40 mM MgCl2, 0.3 mM T7 template, 0.3 mM DNA templates, and 3 mg/ml T7 polymerase. The reaction was performed at 37°C for 4 h. After transcription, the transcription products were treated with 0.1 total volume (0.1 V) of 0.5 M EDTA, 0.1 V of 5 M NaCl, and 3 V of absolute alcohol and incubated at −40°C overnight. The transcription products were then centrifuged, the supernatant was discarded, and the precipitated RNA was dissolved in 1.5 ml of DEPC-treated water. An equal volume of RNA loading buffer (TaKaRa Bio Inc.) was added, and the mixture was incubated at 90°C for 5 min and cooled on ice for 5 min. The RNA samples were separated on a 12% denaturing polyacrylamide gel and purified using Elutrap (Whatman). The final meiRNA was dialyzed against DEPC-treated water and stored at −80°C.

EMSA

EMSA was used to identify the interaction of meiRNA (1–508 nt) and Mei2 RRM3. Different amounts of Mei2 protein (0–12.8 μM) were incubated at 30°C for 20 min in gel-shift buffer (10 mM Tris–HCl, pH 8.0, 25 mM NaCl, 0.1 mM EDTA, 0.1 mg/ml tRNA, and 5 μg/ml heparin). Then, 2 pmol ^{32}P-labelled meiRNA was added to the reaction mixture and incubated at 37°C for 15 min. The mixture was loaded onto an 8% polyacrylamide gel. Gels were run at 120 V for 2 h in 1× TBE buffer and exposed for imaging with a Typhoon FLA 7000 scanner (GE Healthcare).

CLIP–seq in vitro

CLIP–seq was performed as previously described (Xue et al., 2009), with some modifications. Briefly, 6×His-tagged Mei2 RRM3 protein and meiRNA were incubated in binding buffer (10 mM Tris–HCl, pH 8.0, 25 mM NaCl, 0.1 mM EDTA, 0.1 mg/ml tRNA, and 5 μg/ml heparin) and then irradiated at 400 mJ/cm^2 with 254 nm UV light. Dynabeads^{TM} His-Tag (Thermo Fisher Scientific; Catalog # 10103D) was applied to pull down protein–RNA complexes. After micrococcal nuclease treatment and 3′ DNA adaptor ligation (Zarnegar et al., 2016), the immunoprecipitated complexes were fractionated on 4%–12% NuPAGE Bis–Tris gels and transferred to nitrocellulose membranes. The Mei2 RRM3-specific smear bands were excised with scalpels and treated with proteinase K (TaKaRa Bio Inc.; Catalog # 9034) before extracting RNA by phenol and chloroform. A 5′ RNA linker was then added to the isolated RNA, which was reverse-transcribed by superscript reverse transcriptase III (Life Technologies; Catalog # 18080-051). After PCR amplification and deep sequencing, the sequenced reads were first trimmed by removing the 5′- and 3′-adaptor sequences and then mapped to the meiRNA sequence using Bowtie2 (Langmead and Salzberg, 2012). Two mismatches were allowed for mapping. CLIP–seq peaks were identified by Piranha version 1.2.1 with the following parameters: -s -b 20 -d Zero Truncated Negative Binomial -p 1e-5 or 2e-3 (Uren et al., 2012). Supplementary Table S2 summarizes the statistics for *in vitro* CLIP–seq.

FP assay

The lyophilized 5′-FAM-labelled RNA oligomer was purchased from TaKaRa Bio Inc., dissolved in DEPC-treated water to a final concentration of 100 μM, and stored at −80°C. The stock (100 μM) was diluted to 120 nM in buffer C (20 mM Bis–Tris–HCl, pH 6.5, and 150 mM NaCl). Mei2 RRM3 constructs were first diluted to 20 times the highest concentration used in the binding system and then successively diluted 2-fold to reach the lowest desired concentration. Before the FP assay, 100 μl of 120 nM fluorescence-labelled RNA was mixed with 100 μl of protein stocks from the diluted series and incubated for 15 min. Samples were then excited at 485 nm, and the FP was detected at 525 nm using a SpectraMax M5 plate reader (Molecular Devices) at 20°C. All FP data were fitted in a 1:1 binding model well and were expressed as follows:

$$FP = FP_{ini} + \frac{FP_{max}}{2nR} + \left(K_D + P + nR - \frac{FP_{max}}{2nR}\sqrt{-4nRP + (K_D + P + nR)^2}\right),$$

where FP is the observed total polarization, FP_{ini} is the initial FP of RNA with no protein, FP_{max} is the maximum fluorescence polarization, P is the protein concentration, R is the concentra-

tion of labelled RNA, n is the binding stoichiometry (protein:RNA ratio), and K_D is the equilibrium dissociation constant. Standard errors were obtained by fitting the data to the above equation. Supplementary Table S3 summarizes the FP statistics.

SEC–MALS

Two hundred microliters of apoMei2 RRM3 protein and Mei2 RRM3 in complex with 8mer meiRNA at 1 mg/ml were injected into a Superdex 75 Increase 10/300 GL column at a flow rate of 0.3 ml/min in buffer C (20 mM Bis–Tris–HCl, pH 6.5, and 150 mM NaCl) using an ÄKTA purifier. The system was coupled online to an 8-angle MALS detector (DAWN HELEOS II, Wyatt Technology) and a differential refractometer (Optilab T-rEX, Wyatt Technology). Data were analyzed using ASTRA 7.0.1.24.

Plasmids and yeast strains

Supplementary Table S4 lists the plasmids used in this study. For generating pJK148-P*mei2-mei2*-13myc (pCF.3986), the *mei2* promoter (P*mei2*, 1500 base pairs upstream of the start codon of *mei2*) was inserted into the pJK148 vector (pCF.3317). Fission yeast strains used in this study are listed in Supplementary Table S5. Long primers created deletion strains with pFA6a plasmids. Forward-oligo: 5′-AGTCATTAAGTAATTTTTTTTACTCTTTATCTATTTTAAGGATTATCGGCCAGCTTTATTGTTGCCGTTTTAACACATAACGGATCCCCGGGTTAATTAA-3′; Reverse oligo: 5′-TTGAACAAAAATAAAATATAGAAAAGAAAGGGTAAGCAAAGCGATAGGTAAACATAAACAATACAGGATCTCTTTCGTAAGAATTCGAGCTCGTTTAAAC-3′.

Microscopy and data analysis

Imaging was performed as previously described (Zheng et al., 2020), with some modifications. Imaging in this study was performed using a PerkinElmer UltraVIEW Vox spinning-disk microscope equipped with a Hamamatsu C9100-23B EMCCD camera and a CFI Apochromat TIRF 100× objective (NA = 1.49). For confocal imaging, the ME medium containing 3% agar was solidified on a glass slide, and 0.5 μl cells were placed on top of the agar and covered with a coverslip. Cells with opposite mating types were first streaked on yeast extract (YE) plates and grown overnight at 30°C. The fresh cells with opposite mating types from the YE plates were then mixed on ME plates at 30°C. Cells were collected from the ME plates and suspended in the ME liquid medium. For imaging of karyogamy, cells were collected at 10 h after mixing. For spore observation, cells were collected at 24 h after mixing. All media were purchased from Formedium. Cells were imaged with an 11 Z-stack at intervals of 0.5 μm. Data analysis was performed using MetaMorph (Molecular Devices) and ImageJ (Schneider et al., 2012) with the MTrackJ plug-in (National Institutes of Health).

Western blotting

Cell lysates were prepared in lysis buffer (50 mM Tris–HCl, pH 8.0, 150 mM NaCl, and 5 mM EDTA) supplemented with protease inhibitor cocktails (Roche Diagnostics). Equal amounts of total protein were separated using sodium dodecyl sulphate polyacrylamide gel electrophoresis (SDS–PAGE). The primary antibody against Myc was used to test the expression of Mei2-Myc. Tubulin served as a loading control. Horseradish peroxidase-conjugated anti-rabbit and anti-mouse secondary antibodies (Bio-Rad) were used to detect the primary antibody binding, and signals were detected using Western ECL substrate (Bio-Rad).

Measurement of gene expression

Gene expression was measured after 10.5 h. Total RNA was extracted using Trizol reagent (Invitrogen), and reverse transcription was performed using HiScript III RT SuperMix for qPCR (Vazyme Biotech Co. Ltd.). The cDNA samples were subjected to qPCR with SYBR green dye (TaKaRa Bio Inc.) using specific primers (primer information is provided in Supplementary Table S6). Each experiment was repeated at least three times. Expression levels were normalized to the gene *tubulin*. The expression level of each gene in the mutant strain was normalized to the corresponding gene expression level in the wild-type strain. Standard deviations (SDs) within each experiment were calculated.

GST pull-down assay

Hundred micrograms of GST-tagged Mei2$^{571–750}$ or Mei2$^{580–733}$ protein was incubated with GST resin (GE Healthcare) in buffer C (20 mM Bis–Tris–HCl, pH 6.5, 150 mM NaCl) at 4°C for 2 h. GST resin was washed three times with buffer C to remove excess protein. Fifty micrograms of Erh1 were added and mixed on a shaker for 2 h. Unbound Erh1 was washed four times. Results were observed by SDS–PAGE.

Date availability

The atomic coordinates and structure factors for the apoMei2 RRM3 and Mei2 RRM3–meiRNA complex structures have been deposited to the Protein Data Bank (PDB) under the accession codes PDB: 7EIO and PDB: 7EIU, respectively.

Supplementary material

Supplementary material is available at *Journal of Molecular Cell Biology* online.

Acknowledgements

We thank Prof. Yuanchao Xue (Institute of Biophysics, Chinese Academy of Sciences), Prof. Maikun Teng, Prof. Qingguo Gong, Dr Lin Cheng, and Zheng Xu (University of Science and Technology of China) for participating in helpful discussions. We thank the staff of the BL19U1 beamline at the National Center for Protein Science Shanghai and the Shanghai Synchrotron Radiation Facility (Shanghai, China) for assistance during data collection.

Funding

This work was financially supported by grants from the Ministry of Science and Technology of China (2019YFA0508403), the Strategic Priority Research Program of the Chinese Academy of Sciences (XDB39010300), the National Natural Science Foundation of China (32090040, 31870760, 32171222, 92149302, U1932122, and 32100958), the China Postdoctoral Science

Foundation (2019M662182), and the Fundamental Research Funds for the Central Universities (WK2340000097).

Conflict of interest: none declared.

Author contributions: S.S. performed protein expression, crystallographic experiments, and biochemical experiments with the help of M.L. and Y.L., and Z.C. performed *in vitro* CLIP–seq experiments. Y.J. generated fission yeast cell lines and performed *in vivo* experiments and analysis. S.S. designed the structural studies and determined the structure. S.S., Y.J., J.W., F.L., C.F., and Y.S. analyzed the data and wrote the manuscript.

References

Adams, P.D., Afonine, P.V., Bunkoczi, G., et al. (2010). PHENIX: a comprehensive Python-based system for macromolecular structure solution. Acta Crystallogr. D Biol. Crystallogr. *66*, 213–221.

Andric, V., Nevers, A., Hazra, D., et al. (2021). A scaffold lncRNA shapes the mitosis to meiosis switch. Nat. Commun. *12*, 770.

Auweter, S.D., Fasan, R., Reymond, L., et al. (2006). Molecular basis of RNA recognition by the human alternative splicing factor Fox-1. EMBO J. *25*, 163–173.

Chikashige, Y., Ding, D.Q., Funabiki, H., et al. (1994). Telomere-led premeiotic chromosome movement in fission yeast. Science *264*, 270–273.

Chikashige, Y., Ding, D.Q., Imai, Y., et al. (1997). Meiotic nuclear reorganization: switching the position of centromeres and telomeres in the fission yeast Schizosaccharomyces pombe. EMBO J. *16*, 193–202.

Clery, A., Blatter, M., and Allain, F.H. (2008). RNA recognition motifs: boring? Not quite. Curr. Opin. Struct. Biol. *18*, 290–298.

Dominguez, C., and Allain, F.H. (2006). NMR structure of the three quasi RNA recognition motifs (qRRMs) of human hnRNP F and interaction studies with Bcl-x G-tract RNA: a novel mode of RNA recognition. Nucleic Acids Res. *34*, 3634–3645.

Emsley, P., Lohkamp, B., Scott, W.G., et al. (2010). Features and development of Coot. Acta Crystallogr. D Biol. Crystallogr. *66*, 486–501.

Gibeaux, R., and Knop, M. (2013). When yeast cells meet, karyogamy! Nucleus *4*, 182–188.

Harigaya, Y., Tanaka, H., Yamanaka, S., et al. (2006). Selective elimination of messenger RNA prevents an incidence of untimely meiosis. Nature *442*, 45–50.

Harigaya, Y., and Yamamoto, M. (2007). Molecular mechanisms underlying the mitosis–meiosis decision. Chromosome Res. *15*, 523–537.

Hennig, J., Militti, C., Popowicz, G.M., et al. (2014). Structural basis for the assembly of the Sxl–Unr translation regulatory complex. Nature *515*, 287–290.

Horie, S., Watanabe, Y., Tanaka, K., et al. (1998). The Schizosaccharomyces pombe mei4^{+} gene encodes a meiosis-specific transcription factor containing a forkhead DNA-binding domain. Mol. Cell. Biol. *18*, 2118–2129.

Kaur, J., Sebastian, J., and Siddiqi, I. (2006). The Arabidopsis-mei2-like genes play a role in meiosis and vegetative growth in Arabidopsis. Plant Cell *18*, 545–559.

Kitamura, K., Katayama, S., Dhut, S., et al. (2001). Phosphorylation of Mei2 and Ste11 by Pat1 kinase inhibits sexual differentiation via ubiquitin proteolysis and 14-3-3 protein in fission yeast. Dev. Cell *1*, 389–399.

Langmead, B., and Salzberg, S.L. (2012). Fast gapped-read alignment with Bowtie 2. Nat. Methods *9*, 357–359.

Lv, M., Yao, Y., Li, F., et al. (2019). Structural insights reveal the specific recognition of roX RNA by the dsRNA-binding domains of the RNA helicase MLE and its indispensable role in dosage compensation in Drosophila. Nucleic Acids Res. *47*, 3142–3157.

McCoy, A.J., Grosse-Kunstleve, R.W., Adams, P.D., et al. (2007). Phaser crystallographic software. J. Appl. Crystallogr. *40*, 658–674.

Mata, J., and Bahler, J. (2006). Global roles of Ste11p, cell type, and pheromone in the control of gene expression during early sexual differentiation in fission yeast. Proc. Natl Acad. Sci. USA *103*, 15517–15522.

Merlini, L., Dudin, O., and Martin, S.G. (2013). Mate and fuse: how yeast cells do it. Open Biol. *3*, 130008.

Mukherjee, K., Futcher, B., and Leatherwood, J. (2018). mmi1 and rep2 mRNAs are novel RNA targets of the Mei2 RNA-binding protein during early meiosis in Schizosaccharomyces pombe. Open Biol. *8*, 180110.

Murshudov, G.N., Skubak, P., Lebedev, A.A., et al. (2011). REFMAC5 for the refinement of macromolecular crystal structures. Acta Crystallogr. D Biol. Crystallogr. *67*, 355–367.

Navaza, J., and Saludjian, P. (1997). [33] AMoRe: an automated molecular replacement program package. Methods Enzymol. *276*, 581–594.

Niccoli, T., Yamashita, A., Nurse, P., et al. (2004). The p150-Glued Ssm4p regulates microtubular dynamics and nuclear movement in fission yeast. J. Cell Sci. *117*, 5543–5556.

Otsubo, Y., Yamashita, A., Ohno, H., et al. (2014). S. pombe TORC1 activates the ubiquitin–proteasomal degradation of the meiotic regulator Mei2 in cooperation with Pat1 kinase. J. Cell Sci. *127*, 2639–2646.

Otwinowski, Z., and Minor, W. (1997). Processing of X-ray diffraction data collected in oscillation mode. Methods Enzymol. *276*, 307–326.

Sato, M., Shinozaki-Yabana, S., Yamashita, A., et al. (2001). The fission yeast meiotic regulator Mei2p undergoes nucleocytoplasmic shuttling. FEBS Lett. *499*, 251–255.

Schneider, C.A., Rasband, W.S., and Eliceiri, K.W. (2012). NIH Image to ImageJ: 25 years of image analysis. Nat. Methods *9*, 671–675.

Shichino, Y., Otsubo, Y., Kimori, Y., et al. (2018). YTH-RNA-binding protein prevents deleterious expression of meiotic proteins by tethering their mRNAs to nuclear foci. eLife *7*, e32155.

Shichino, Y., Yamashita, A., and Yamamoto, M. (2014). Meiotic long noncoding meiRNA accumulates as a dot at its genetic locus facilitated by Mmi1 and plays as a decoy to lure Mmi1. Open Biol. *4*, 140022.

Shimada, T., Yamashita, A., and Yamamoto, M. (2003). The fission yeast meiotic regulator Mei2p forms a dot structure in the horse-tail nucleus in association with the sme2 locus on chromosome II. Mol. Biol. Cell *14*, 2461–2469.

Shimoda, C., Uehira, M., Kishida, M., et al. (1987). Cloning and analysis of transcription of the mei2 gene responsible for initiation of meiosis in the fission yeast Schizosaccharomyces pombe. J. Bacteriol. *169*, 93–96.

Skrisovska, L., Bourgeois, C.F., Stefl, R., et al. (2007). The testis-specific human protein RBMY recognizes RNA through a novel mode of interaction. EMBO Rep. *8*, 372–379.

Stoilov, P., Rafalska, I., and Stamm, S. (2002). YTH: a new domain in nuclear proteins. Trends Biochem. Sci. *27*, 495–497.

Sugiyama, T., Thillainadesan, G., Chalamcharla, V.R., et al. (2016). Enhancer of rudimentary cooperates with conserved RNA-processing factors to promote meiotic mRNA decay and facultative heterochromatin assembly. Mol. Cell *61*, 747–759.

Uren, P.J., Bahrami-Samani, E., Burns, S.C., et al. (2012). Site identification in high-throughput RNA–protein interaction data. Bioinformatics *28*, 3013–3020.

Vagin, A., and Teplyakov, A. (2010). Molecular replacement with MOLREP. Acta Crystallogr. D Biol. Crystallogr. *66*, 22–25.

Wang, C., Zhu, Y., Bao, H., et al. (2016). A novel RNA-binding mode of the YTH domain reveals the mechanism for recognition of determinant of selective removal by Mmi1. Nucleic Acids Res. *44*, 969–982.

Watanabe, Y., Lino, Y., Furuhata, K., et al. (1988). The S. pombe mei2 gene encoding a crucial molecule for commitment to meiosis is under the regulation of cAMP. EMBO J. *7*, 761–767.

Watanabe, Y., and Nurse, P. (1999). Cohesin Rec8 is required for reductional chromosome segregation at meiosis. Nature *400*, 461–464.

Watanabe, Y., Shinozaki-Yabana, S., Chikashige, Y., et al. (1997). Phosphorylation of RNA-binding protein controls cell cycle switch from mitotic to meiotic in fission yeast. Nature *386*, 187–190.

Watanabe, Y., and Yamamoto, M. (1994). S. pombe mei2^{+} encodes an RNA-binding protein essential for premeiotic DNA synthesis and

meiosis I, which cooperates with a novel RNA species meiRNA. Cell *78*, 487–498.

Wu, B., Xu, J., Su, S., et al. (2017). Structural insights into the specific recognition of DSR by the YTH domain containing protein Mmi1. Biochem. Biophys. Res. Commun. *491*, 310–316.

Xie, G., Vo, T.V., Thillainadesan, G., et al. (2019). A conserved dimer interface connects ERH and YTH family proteins to promote gene silencing. Nat. Commun. *10*, 251.

Xue, Y., Zhou, Y., Wu, T., et al. (2009). Genome-wide analysis of PTB–RNA interactions reveals a strategy used by the general splicing repressor to modulate exon inclusion or skipping. Mol. Cell *36*, 996–1006.

Yamamoto, M. (1996a). The molecular control mechanisms of meiosis in fission yeast. Trends Biochem. Sci. *21*, 18–22.

Yamamoto, M. (1996b). Regulation of meiosis in fission yeast. Cell Struct. Funct. *21*, 431–436.

Yamamoto, M. (2010). The selective elimination of messenger RNA underlies the mitosis–meiosis switch in fission yeast. Proc. Jpn Acad. Ser. B Phys. Biol. Sci. *86*, 788–797.

Yamanaka, S., Yamashita, A., Harigaya, Y., et al. (2010). Importance of polyadenylation in the selective elimination of meiotic mRNAs in growing S. pombe cells. EMBO J. *29*, 2173–2181.

Yamashita, A., Sakuno, T., Watanabe, Y., et al. (2017). Analysis of Schizosaccharomyces pombe meiosis. Cold Spring Harb. Protoc. *2017*, pdb.top079855.

Yamashita, A., Shichino, Y., Tanaka, H., et al. (2012). Hexanucleotide motifs mediate recruitment of the RNA elimination machinery to silent meiotic genes. Open Biol. *2*, 120014.

Yamashita, A., Watanabe, Y., Nukina, N., et al. (1998). RNA-assisted nuclear transport of the meiotic regulator Mei2p in fission yeast. Cell *95*, 115–123.

Yamashita, A., Watanabe, Y., and Yamamoto, M. (1997). Microtubule-associated coiled-coil protein Ssm4 is involved in the meiotic development in fission yeast. Genes Cells *2*, 155–166.

Zarnegar, B.J., Flynn, R.A., Shen, Y., et al. (2016). irCLIP platform for efficient characterization of protein–RNA interactions. Nat. Methods *13*, 489–492.

Zheng, F., Dong, F.F., Yu, S., et al. (2020). Klp2 and Ase1 synergize to maintain meiotic spindle stability during metaphase I. J. Biol. Chem. *295*, 13287–13298.

Zofall, M., Yamanaka, S., Reyes-Turcu, F.E., et al. (2012). RNA elimination machinery targeting meiotic mRNAs promotes facultative heterochromatin formation. Science *335*, 96–100.